Petroleum Science 23 (2026) 5221–5233

Contents lists available at ScienceDirect

Petroleum Science

journal homepage: www.keaipublishing.com/en/journals/petroleum-science

Original Paper

Co-pyrolysis of oil shale and bituminous coal in a fluidized bed: Properties and distribution of pyrolysates, and reaction mechanisms

Dong-Ling Xu, Yue Ma, Zhi-Jun Fu, Lu Gong, Ze-Kai Zhang, Hao-Lun Wang, Jin-Ke Wang, Feng-Zhi Guo, Si-Jia Li, Ke-Xin Zhao, Chang-Tao Yue *

State Key Laboratory of Heavy Oil Processing, China University of Petroleum (Beijing), Beijing, 102249, China

ARTICLE INFO

Article history:
Received 6 October 2025
Received in revised form
26 November 2025
Accepted 25 March 2026
Available online 27 March 2026

Edited by Min Li

Keywords:
Oil shale
Bituminous coal
Fluidized bed
Co-pyrolysis
Pyrolysates
Cracking mechanism

ABSTRACT

The co-pyrolysis of mixed samples of Longkou oil shale (OS) and bituminous coal (BC), using the ash of the mixture as the heat carrier, was investigated in a fluidized bed. The influencing factors were determined, including temperature, particle size, nitrogen flow rate, and heating rate. With the effect of modulating volatile residence time and secondary reaction severity, the basic properties and distribution of pyrolysates were obtained. Among them, temperature was the most critical factor. The yield of pyrolysis oil increased initially and then decreased with rising temperature, reaching a maximum of 20.95 wt.% and the yield of pyrolysis gas from cracking was suppressed to 10.67 wt.% under the optimized conditions of 520 °C, a particle size of 0.7–1.0 mm, and a nitrogen flow rate of 0.6 L/min. The relative content of alkane in the pyrolysis oil was decreased from 55.90% to 41.33%, while the relative contents of olefins, aromatics, and phenols were increased. At the same time, the yields of CH_4 and H_2 were also increased according to the intensified secondary reactions. The analysis of synergistic effect indicated that the addition of OS diluted the alkali/alkaline earth metals in the system, which effectively inhibited cross-linking and coking, promoted the release of aromatic structures and the yield of phenols in pyrolysis oil increased from 1.27 wt.% to 1.75 wt.%. This study confirmed that secondary cracking during co-pyrolysis was mainly driven by free radical chain reactions, which promoting the carbon of pyrolysis gas and pyrolysis oil lower.

1. Introduction

According to projections by the International Energy Agency (IEA), global energy consumption is projected to increase by 15% between 2023 and 2030, requiring a strong focus on scaling up oil and gas processing capacity to meet the growing demand. (Wang et al., 2024). Global reserves include extensive deposits of oil shale and low-rank coal, making improving their utilization efficiency a critical priority in the energy and chemical industries (Wang et al., 2025). Pyrolysis, a key technology for value-added utilization, transforms 60%–70% of organic matter into liquid fuels and chemicals and is widely used in the utilization of oil shale and low-rank coal (Xiong et al., 2025). Oil shale is a combustible sedimentary rock with high inorganic mineral content and low yields of pyrolysis oil and pyrolysis gas (Shu et al., 2025). The shale oil has high viscosity and elevated nitrogen and sulfur content (S. Cui et al., 2024). Low-rank coal, which includes lignite and low-metamorphic bituminous coal, is characterized by high moisture content, low ash content, high carbon and low hydrogen content (Ma et al., 2023). The coal tar obtained through low-temperature distillation of low-rank coal contains high levels of sulfur, nitrogen, and other heteroatoms, along with numerous phenols, polycyclic aromatics, furans, and oxygenated compounds, as well as aromatic carbon compounds, resulting in poor quality of coal tar (Gao et al., 2021).

In recognition of the inherent limitations associated with pyrolysates derived from oil shale and low-rank coal, scholars have begun exploring the feasibility of mixed pyrolysis of these two resources in recent years (Zhu et al., 2025). Oil shale, characterized by a high hydrogen-to-carbon ratio, has the potential to supply hydrogen radicals during co-pyrolysis with low-rank coal (Zhai et al., 2023), thereby addressing the issue of poor quality in low-rank coal tar and enhancing both the calorific value and stability of the resulting mixed pyrolysis oil. Furthermore, co-pyrolysis can

* Corresponding author.
E-mail address: yuect@cup.edu.cn (C.-T. Yue).
Peer review under the responsibility of China University of Petroleum (Beijing).

https://doi.org/10.1016/j.petsci.2026.03.058

mitigate the reduction in the yields of pyrolysis oil and pyrolysis gas caused by the high mineral content in oil shale (Bhattacharyya et al., 2024). Notably, oil shale deposits are frequently found alongside coal in regions such as Longkou, Yaojie, and Fushun in China (Zhou et al., 2020). The advancement of co-pyrolysis technology for oil shale and coal can reduce costs associated with separate mining and pretreatment processes, aligning with the principles of the circular economy. This study focuses on the co-pyrolysis process of Longkou oil shale and its associated low-rank bituminous coal. By optimizing the pyrolysis conditions, this approach can lead to multiple synergistic benefits, including increased oil yield, reduced coke formation, improved oil quality and cost reduction, thereby providing a new approach for the efficient utilization of oil shale and low-rank coal (Niu et al., 2024; Wu et al., 2022).

During the co-pyrolysis of oil shale and lignite, a synergistic effect was observed. At a 50% oil shale mixing ratio, the increase in the yields of pyrolysis oil and pyrolysis gas reached its maximum, exceeding the theoretical value by 1.4 wt.% (Li et al., 2016). Under equivalent conditions, low-rank coal with high volatile matter, low moisture, and low ash content exhibits a synergistic effect with oil shale during pyrolysis. Specifically, weight loss due to hydrocarbon release in mixed samples occurred primarily between 350 and 550 °C (Miao et al., 2012). Co-pyrolysis of biomass and low-rank coal increased yields of gaseous and liquid products while reducing semi-coke. Lu et al. (2020) confirmed a synergistic effect during co-pyrolysis of 95 wt.% oil shale and 5 wt.% coal, and the yields of oil and gas increased by 8.20% and 2.65%, respectively (Bhattacharyya et al., 2024).

Furthermore, phenolic compounds, recognized as high-value-added chemicals, exhibit a formation pathway and regulatory mechanism during co-pyrolysis that remains elusive. During the co-pyrolysis of oil shale and peanut shell phenolic compounds undergo further transformation into aromatic compounds through catalytic alkylation transfer and dehydration of methoxy groups on the benzene ring (Z. Cui et al., 2024). Phenol was primarily generated through the pyrolysis of oxygen-containing macromolecules in coal, and inherent minerals CaO and Fe_2O_3 in coal could promote the cleavage of catechol side chains (Bai et al., 2014).

In current industrial practices, solid heat carrier technology is employed to enhance heating efficiency in the pyrolysis of oil shale and coal, as exemplified by methods such as the Galoter retort (Stelmakh and Tyagunov, 1986) and Alberta Taciuk retort (Kılıç et al., 2014) for oil shale retorting, and Toscoal retort (Huang et al., 2017), and Lurgi-Ruhr (Röpke and Peyrer, 1980) for coal retorting. The prevalent types of solid heat carriers employed include ceramic balls, quartz sand, ash of coal or oil shale (Li et al., 2024). Remarkably, ash of coal or oil shale acted as a solid heat carrier, exhibiting efficient heat storage and transfer capabilities, which enhance yield of pyrolysis oil. Furthermore, the inorganic constituents within ash such as silicates, carbonates, quartz, and minor quantities of pyrite, significantly influence the pyrolysis process, thereby affecting the yields and characteristics of pyrolysis oil and pyrolysis gas (Zhang et al., 2023). Ash of oil shale enhanced yields of pyrolysis oil and pyrolysis gas of Huadian oil shale. Additionally, the aliphatic contents in pyrolysis oil decreased, accompanied by shortened aliphatic chain lengths and increased contents of aromatics (Shi et al., 2017). During high-temperature coal pyrolysis, CaO can catalyze CH_4 formation from carbon oxides and organic carbon when H_2 is abundant. Silicate minerals provided acidic sites that facilitate decarboxylation and aliphatic hydrocarbon cleavage (Wu et al., 2024).

The pyrolysis oil generated during the pyrolysis of coal, oil shale and other organic substances underwent further transformations at elevated temperatures to produce gas, coke and oil. This phenomenon is termed as secondary reactions, and they affect the properties and distribution of pyrolysates (Zhai et al., 2015). Factors such as temperature, particle size, reaction atmosphere, nitrogen flow rate, reaction duration, and catalyst governed the extent of secondary reactions in pyrolysis oil. Amer et al. The density of shale oil increased as the final reaction temperature increased from 360 to 500 °C. Furthermore, the average molecular weight of sulfides and heavy oil fraction in shale oil at 520 °C exceeded those at 460 °C (Amer et al., 2019). A positive correlation between temperature and the conversion of organic carbon was observed in coal (Kareemulla et al., 2024). The impact of particle size on coal pyrolysis was investigated using Fourier Transform Infrared Spectroscopy (FTIR) and Thermogravimetric Analysis (TGA). The results demonstrated that CH_4, aliphatic hydrocarbons and light aromatics decreased progressively with reduced particle size, whereas CO remained unchanged (Chen et al., 2018). Introducing water vapor into the pyrolysis atmosphere of Huadian oil shale and microalgae enhanced the yield of pyrolysis oil reduced the contents of phenols, mono-aromatics and polycyclic aromatic hydrocarbons (PAHs), and then improved the quality of pyrolysis oil (Chang et al., 2023). Increasing the N_2 flow rate from 20 to 100 mL/min during the pyrolysis of lignin raised bio-oil yield from 1.18% to 8.20%. However, at 150 mL/min, bio-oil yield decreased to 5.12%. Higher N_2 flow rates facilitated rapid removal of pyrolysis products, enabling organic macromolecules to form coke (Wulandari et al., 2020). The yield of pyrolysis oil during the pyrolysis of polystyrene waste initially increased and then stabilized with prolonged reaction time (Miandad et al., 2016).

Based on previous research, pyrolysis reactors are classified into fixed bed, moving bed, fluidized bed, Rotary kiln and other reactor types (Qian et al., 2019). Using two fluidized bed reactors, the effect of the char-to-coal mass ratio on pyrolysis was investigated when char served as the solid heat carrier. The research showed that increasing ratio enhanced the yields of pyrolysis oil and pyrolysis gas while reduced production of semi-coke. The content of light component in the pyrolysis oil increased, thereby improving its quality (Li et al., 2024). An investigation into the co-pyrolysis of low-rank bituminous coal with algal biomass was conducted in a rotary kiln reactor. The findings revealed that as temperature increased, the concentration of PAHs and polycyclic aromatic nitrogen hydrocarbons (PANHs) in pyrolysis oil significantly decreased (Nyoni and Hlangothi, 2023). The microwave co-pyrolysis of textile dyeing sludge (TS) and furfural residue (FR) was investigated. The addition of FR neutralized the strong alkalinity of the bio-oil, facilitating the enrichment of C and H in the biochar and increasing the calorific value (Liu et al., 2024). The effect of coal gangue (CG) on the pyrolysis of oily sludge using a fixed bed. The results showed that for catalytic pyrolysis, the selectivity of aromatics in the pyrolysis oil was 97.55%, and naphthalene compounds accounted for 55.75% of the total aromatics (Liu et al., 2025a,b).

Previous studies had predominantly focused on the blending ratio of oil shale to coal and the individual pyrolysis behaviors of each fuel. And the specific operational parameters for the co-pyrolysis of mixture, especially in fluidized bed reactor remained insufficiently explored. In this manuscript, co-pyrolysis of the mixture of oil shale and bituminous coal were carried out in a fluidized bed using the ash of mixture as the solid heat carrier, leveraging the endogenous synergy of the materials and the active regulation of secondary reactions. The effects of reaction temperature, particle size, nitrogen flow rate and heating rate on properties and distribution of final pyrolysates were investigated. The cracking mechanism of organic macromolecules during the process of co-pyrolysis, especially the secondary reactions were

investigated. Moreover, the formation mechanism of phenolic substances during co-pyrolysis of the mixture was explored. This research could provide important insights for industrial applications of co-pyrolysis of oil shale and bituminous coal.

2. Experimental

2.1. Material

The oil shale (OS) and bituminous coal (BC) samples were collected from Longkou, Shandong Province, China. The samples were first pretreated by grinding and sieving, and then the fraction of particle size less than 0.2 mm was selected for subsequent experimental analyses which including proximate analysis (GB/T 212-2008), Fischer assay analysis (GB/T 480-2010) and ultimate analysis (Vario MICRO cube, Germany) and ash composition analysis (ARL Advant X Intellipower TM 3600, United States). The results were summarized in Tables 1 and 2.

As illustrated in Table 1, the ash content of OS amounted to 39.39 wt.%, markedly exceeding that of BC. In contrast, the volatile matter content of both samples exhibited similarity, with values of 33.57 wt.% and 35.40 wt.%, respectively. It was worth noting that the fixed carbon content of BC stood at 52.08 wt.%, substantially higher than that of OS. OS and BC undergo Fischer assay analysis, yielding pyrolysis water, pyrolysis oil, pyrolysis gas and semi-coke. Among them, the yield of oil from OS was as high as 16.33 wt.%, and that from BC was only 6.54 wt.%. The yields of semi-coke were comparable between OS and BC, 68.26 wt.% and 65.64 wt.%, respectively. However, BC exhibited a substantially higher pyrolysis gas yield compared to OS. The ultimate analysis revealed that the H/C ratio of BC was 0.92, which was lower than that of OS. This observation suggested that the pyrolysis oil derived from BC contained a greater proportion of unsaturated components compared to the pyrolysis oil from OS.

Moreover, the oxygen content within BC attained a significant level of 24.66 wt.%, subsequently leading to an increased proportion of oxygen-containing compounds in its pyrolysis oil. Consequently, the quality of pyrolysis oil obtained from BC proved to be comparatively lower than that derived from OS. The co-pyrolysis of BC and OS had emerged as a potential method for adjusting the component of the pyrolysates and improving the quality of the resulting oil. As demonstrated in Table 2, the concentrations of CaO, Na_2O, and MgO in BC were markedly higher than those in OS. This compositional difference likely played a role in facilitating the catalytic activity of these alkali metals and alkaline earth metals during the co-pyrolysis process of BC and OS (Liu et al., 2025a, 2025b; Zhao et al., 2021).

2.2. Thermogravimetric experiments

The pyrolysis behaviors of OS, BC, and their mixture (the weight rate of OS in mixture was 60%), were individually investigated with a Shimadzu TGA-50 thermogravimetric analyzer. The samples were weighted 20 ± 0.2 mg. The TG experiments were carried out at a heating rate of 200 °C/min from room temperature to 800 °C under a nitrogen atmosphere (50 mL/min).

Table 2
XRF analysis of OS and BC (dry basis), wt.%.

Composition	SiO_2	Al_2O_3	CaO	Fe_2O_3	SO_3	Na_2O	K_2O	MgO
OS	74.61	6.57	6.41	4.40	2.93	2.53	0.59	0.45
BC	20.59	18.82	13.01	7.27	20.90	15.18	0.61	1.68

2.3. Pyrolysis experiments in fluidized bed

Fig. 1 depicted the fluidized bed device employed in the rapid pyrolysis experiments. This apparatus comprised a reactor, a temperature controller, an oil and gas condensation unit, and a drainage system for gas collection. The reactor was made of stainless steel, with an inner diameter of 56 mm and a height of 380 mm. It was sealed using flanges and graphite gaskets. A metal filter with a pore size of 20 μm was installed at the top of the vessel. Pyrolysis products passed through the metal filter before entering the oil and gas condensation device, which effectively prevented the escape of fine solid particles. Two rigid channels were embedded at the top of the reactor, extending directly to the bottom. One delivered nitrogen gas, while the other housed a K-type thermocouple for real-time temperature measurement; the readings were displayed on the temperature controller. The side wall of the reactor featured a feeding port for sample introduction. Under nitrogen flow, the sample and heat carrier remained partially fluidized. The oil and gas condensation device consisted of a two-stage series condensation system, using ethanol as the condensing agent at a temperature of −30 ± 1 °C. The drainage gas collection device collected pyrolysis gas while simultaneously measuring their volume through water displacement.

The experiments investigated the effects of temperature, particle size, nitrogen flow rate, and heating rate on the properties and distribution of co-pyrolysates derived from the mixture. The specific parameters and numerical values pertaining to these four influencing factors were presented in Fig. 2.

Before the experiment, 20 g solid heat carrier (prepared from the ash of the mixture after combustion at 815 °C for 4 h) was placed into the reactor, and the carrier gas valve was opened to introduce nitrogen for preheating. When the reactor temperature reached the set point, 10 g mixture was quickly introduced through the feed port, and timing was initiated simultaneously. Pyrolysates were collected after the specified reaction time. These procedures ensured rapid heating of the sample by the fluidized heat carrier, which provided high heat transfer efficiency, minimized secondary reactions, and facilitated subsequent analysis.

The weight of liquid products was measured using weight and subtraction method. The components of pyrolysis oil were

Table 1
The proximate analysis, Fischer assay analysis and ultimate analysis of OS and BC.

Material	Proximate analysis (received basis), wt.%				Fischer assay analysis (dry basis), wt.%			
	Moisture	Ash	Volatile	Fixed carbon	Oil	Water	Semi-coke	Gas
OS	3.01	39.39	33.57	24.03	16.33	7.80	68.26	7.61
BC	6.97	5.55	35.40	52.08	6.54	16.00	65.64	11.22
	Ultimate analysis (dry basis), wt%							H/C
	C	H	O		N		S	
OS	49.09	5.06	12.34		1.51		0.77	1.24
BC	66.96	5.15	24.66		1.89		0.47	0.92

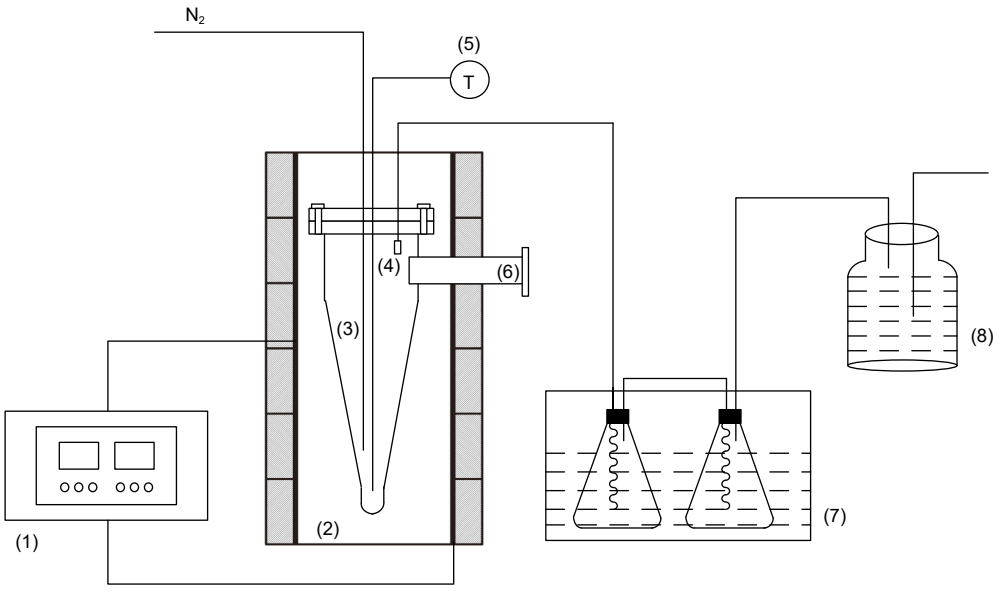

Fig. 1. The fluidized bed pyrolysis device and product collection device. (1) Reactor controller; (2) Open heating furnace; (3) Reaction kettle; (4) Filter; (5) Thermocouple; (6) Feed port; (7) Condensing device; (8) Gas cylinder.

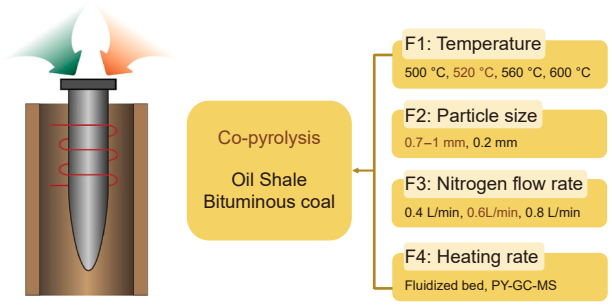

Fig. 2. The schematic diagram of influencing factors investigated in co-pyrolysis experiment.

collected by flushing the condensing unit with methylene chloride, and the water content was determined using distillation method. The mass of pyrolysis gas was obtained by multiplying the gas density by the gas volume, and the gas density was calculated based on the composition of gas. After pyrolysis, the weight of the semi-coke corresponded to the mass of the solid-phase residue minus the solid heat carrier. The solid-phase residue was incinerated in a muffle furnace at a temperature of 815 °C for a duration of 4 h. The difference in mass observed before and after incineration represented coke deposition. The relative content of coke deposition is defined as the ratio of the mass of coke deposition to the semi-coke, whereas the yield of coke deposition is the proportion of the mass of coke deposition to the initial mixture. These two indicators provide a quantitative measure to describe the efficiency of carbon conversion in the investigation.

2.4. Analysis of pyrolysates

The pyrolysis oil was analyzed via GC-MS (Agilent 6890/Bruker Scion TQ instrument). The GC was equipped with HP-5 and HP-5 MS capillary columns. Helium (99.999% purity) served as the carrier gas at a flow rate of 1 mL/min. The column temperature program was as follows: initial temperature 50 °C, increased to 120 °C at 20 °C/min, then to 250 °C at 4 °C/min, and finally to 310 °C at 3 °C/min, where it was held for 30 min. The injection port temperature was 280 °C. The mass spectrometer utilized an electron impact (EI) ionization source with a source temperature of 200 °C, quadrupole temperature of 260 °C, and electron energy of 70 eV. Spectra were matched against the NIST mass spectral library to identify components, and relative contents were calculated from chromatographic peak areas. The pyrolysis oil of the mixture primarily contained alkanes, olefins, aromatic hydrocarbons, phenols, and alcohols. The yield of each component is calculated by multiplying its relative content by the yield of pyrolysis oil. Pyrolysis gas was analyzed using an Agilent 6890n gas chromatograph (GC) with an Agilent 7683 B column. Carrier gas included air (300 mL/min), N_2 (4 mL/min), and H_2 (40 mL/min). The injection port was maintained at ambient temperature, and the detector temperature was 250 °C. The column oven started at 50 °C, held for 3 min, then ramped to 100 °C at 5 °C/min, followed by a second ramp to 180 °C at 10 °C/min and held for 3 min. Detectable gases included H_2, CO_2, CO and C_1–C_5 hydrocarbons. Data processing and analysis were performed using ChemStations Instrument1 Offline software.

2.5. Pyrolysis-gas chromatograph-mass spectrometry

The pyrolysis-gas chromatography/mass spectrometry (Py-GC/MS) system consisted of three main components: a pyrolyzer (CDS 5200 HPR), a gas chromatograph (Agilent 7890 A), and a mass spectrometer (Agilent 5975C). The gas chromatograph was equipped with a 30 m × 0.25 mm × 0.25 μm HP-5MS quartz capillary column, and the injection port temperature was set to 290 °C. An electron impact (EI) ion source was used with an ionization voltage of 70 eV. The mass scanning range was set from 30 to 550 amu (atomic mass units). The oven temperature program was as follows: initial temperature of 50 °C, increased to 120 °C at a rate of 20 °C/min, then to 250 °C at 4 °C/min, and finally to 310 °C at 3 °C/min, followed by a 30-min hold. Nitrogen was used as the carrier gas at a flow rate of 1 mL/min. During pyrolysis, 1 μL of sample was injected into the pyrolyzer using a microsyringe. The gaseous products emerging from the pyrolyzer were mixed with a standard and introduced into the capillary column by a flow of

99.99% helium at a constant rate of 0.8 mL/min, with a split ratio of 50:1.

High-purity helium (99.999 *v*/*v*%) was used as the pyrolysis atmosphere. Mixed samples weighing between 10 and 1000 μg were placed in a metal cup, which was fixed in the waiting zone above the pyrolysis furnace. When the furnace reached the set temperature of 520 °C, the metal cup was dropped into the furnace to initiate rapid pyrolysis. The resulting gaseous products were swept by helium into the gas chromatography system. Compound identification was achieved using the NIST mass spectral database and relevant literature.

3. Results and discussion

3.1. Thermogravimetric analysis

According to Fig. 3, the TG and DTG curves of the samples (OS, BC and their mixture) at a heating rate of 200 °C/min could be divided into three stages, including water removal (100–280 °C), thermal cracking of organic macromolecules (280–600 °C for BC, 280–650 °C for OS) and decomposition of inorganic minerals (600–800 °C for BC, 650–800 °C for OS) (Ding et al., 2022). In the first stage, the weight loss rate of BC was 8.65 wt.%, whereas that of OS was 4.15 wt.% which occurred due to the evaporation of adsorbed water from the internal pores and surface of the particles upon heating. Furthermore, BC exhibited greater superhydrophilicity (Li et al., 2016) than oil shale, a property that was consistent with the proximate analysis results for moisture content. In the second stage, the weight loss rate of OS and BC were 34.59 wt.% and 27.07 wt.%, respectively. In the second stage, the weight loss rates of oil OS and BC were 34.59% and 27.07%, respectively. This stage involved the breakdown of shorter fatty side chains and key fatty bridge bonds within the organic structures. The significantly higher weight loss rate observed for OS, compared to BC, was attributed to the larger proportion of aliphatic structures in OS, as opposed to the more stable aromatic structures predominant in BC. The third stage was observed at approximately 800 °C, where OS, BC, and their mixtures exhibit significant weight-loss. This phenomenon was primarily attributed to the thermal decomposition of inorganic mineral components, such as calcium carbonate, dolomite, within the samples. These findings, supported by prior observations of similar decarbonization-induced weight loss in hydrocarbon-rich materials at high temperatures, confirm this behavior pattern (Fan et al., 2015). In the TG curve, the weight loss of the mixture during the first stage was gradual, while the second stage exhibited a steeper slope, mirroring the weight loss trend of pure oil shale. TG curve showed that in the initial stage, the weight loss curve of the mixture displayed a gradual decline. Subsequently, in the second stage, the slope of this curve steepened significantly, resulting in an overall weight loss trend paralleling that of oil shale. Specifically, the weight loss rates during the second stage were measured at 34.60 wt.% for OS, 20.86 wt.% for BC, and 32.14 wt.% for the mixture. Using a 60% mixing ratio, the theoretical weight loss for the mixture in the second stage was calculated to be 29.10 wt.%. Notably, the experimental value exceeded the theoretical value, suggesting this discrepancy may promote the fragmentation of organic macromolecules in the mixture.

The DTG curve revealed that the primary weight loss for OS, BC, and the mixture occurred in the second stage. The maximum weight loss rates were 0.2632%/°C (OS), 0.1094%/°C (BC), and 0.2128%/°C (mixture). The theoretical maximum weight loss rate of the mixture was 0.2017%/°C calculated based on the oil shale proportion, was lower than the experimental value. This discrepancy confirmed that co-pyrolysis of OS and BC synergistically enhanced organic matter decomposition, likely due to catalytic interactions occurred in the thermal decomposition of the two feedstocks. The H/C ratio of OS was much higher than that of BC, and then during the pyrolysis stage of organic matter, OS could provide H atoms to BC, promote the pyrolysis of organic macromolecules in BC to produce small molecules, inhibit the condensation reaction, which resulted in the reduction of the yield of semi-coke (Song et al., 2021). At the same time, the abundant presence of alkali metals and alkaline earth metals, such as Na and Ca, in BC enhances catalytic activity. This enhancement strengthens the cleavage of chemical bonds in organic components during pyrolysis, thereby improving decomposition efficiency of oil shale (Wang et al., 2022a,b).

3.2. The effect of temperature on the properties and distribution of co-pyrolysates from the mixture

Fig. 4(a) demonstrated the distribution of co-pyrolysates from mixture at different temperatures when particle size was 0.7–1.0 mm, nitrogen flow rate was 0.6 L/min and reaction time was 8 min. As the pyrolysis temperature increased, the yield of

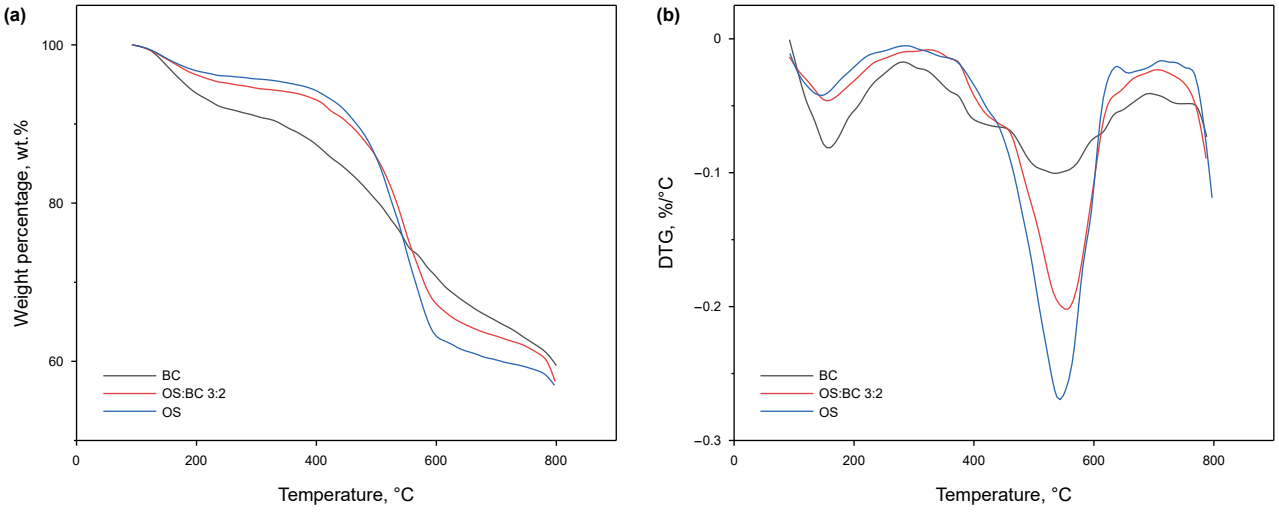

Fig. 3. **(a)** TG curves, **(b)** DTG curves of OS, BC and their blends.

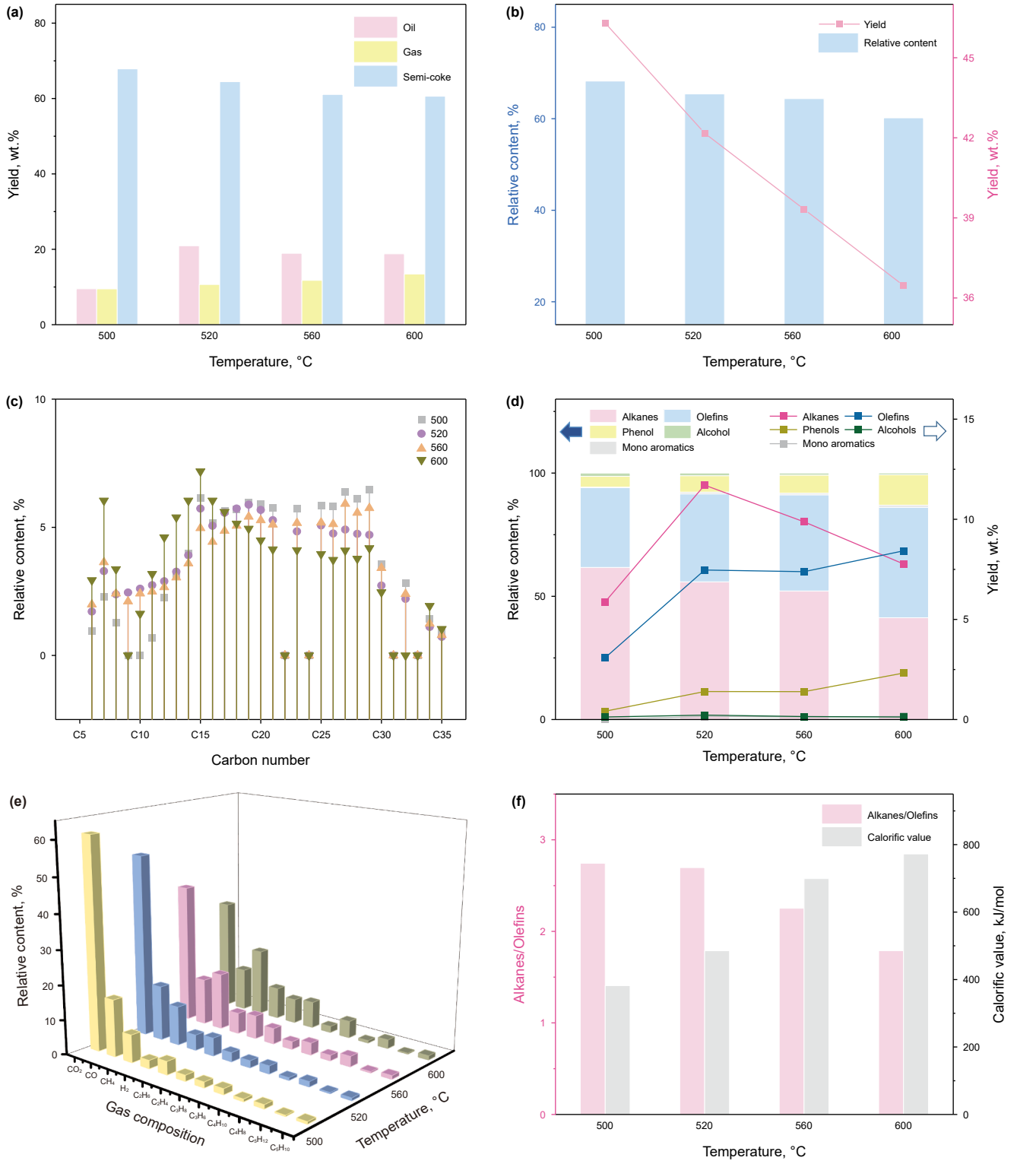

Fig. 4. The effect of temperature on properties and distribution of pyrolysates: **(a)** The distribution of three-phase pyrolysates; **(b)** The relative content and yield of coke deposition; **(c)** The distribution of carbon number; **(d)** The relative content and yield of components in pyrolysis oil; **(e)** The relative content of components in pyrolysis gas; **(f)** The properties of pyrolysis gas.

pyrolysis oil initially rose and subsequently declined, the yield of pyrolysis gas increased, and the yield of semi-coke decreased. When the temperature increased from 500 to 520 °C, the yield of pyrolysis oil peaked at 20.95 wt.%, attributable to the breakdown of organic macromolecular carbon skeletons into fatty and aromatic hydrocarbons. In the range of 520–600 °C, the yield of pyrolysis oil exhibited a gradual decrease, while the yield of pyrolysis gas continued to rise. This trend reflects intensified secondary reactions of pyrolysis oil at higher temperatures, generating light hydrocarbons and nonhydrocarbon gases. Fig. 4(b)

illustrated a steady decline in both the relative content and yield of coke deposition as the temperature increases, suggesting that the coking reaction of heavy oil components was suppressed under these conditions. The polycondensation reactions, which involved the gradual polymerization of aromatics and thick-ringed compounded to form coke precursors, were impacted by the elevated temperatures. Specifically, the high temperatures expedited the secondary reactions of these coke precursors, thereby impeding their stabilization into coke (Zhang et al., 2022).

Fig. 4(c) exhibited the carbon number distribution of pyrolysis oil at different temperatures. With the increase of temperature, the proportion of C_6–C_{12} components increased from 7.5% to 21.76%, the proportion of C_{12}–C_{21} components changed relatively little while the proportion of C_{21+} components decreased from 50.85% to 33.41%. The increasing temperature promoted the further pyrolysis of organic matter in the mixture, releasing a large number of light components, and shifting the carbon number distribution of pyrolysis oil toward low-carbon species (Wang et al., 2016). Fig. 4(d) showed the relative content and yields of alkanes, olefins, aromatic hydrocarbons, phenols and alcohols in the pyrolysis oil at different temperatures. It is evident that alkanes and olefins constituted the majority, and with increasing temperature, the proportion of alkane continued to decrease and the decrement reached 20.41%, while the proportion of olefin continued to increase and the increment was 12.43%. This can be explained by the elevated temperatures facilitated the conversion of long-chain aliphatic hydrocarbons into short-chain alkanes, olefins, and light gases, thereby increasing the proportion of olefins (Kong et al., 2014).

Fig. 4(e) illustrated the pyrolysis gas was mainly composed of C_1–C_5 hydrocarbon gas and inorganic gas components H_2, CO_2, CO. As the temperature increased from 500 to 600 °C, the proportion of CH_4 increased from 8.01% to 19.56%, the proportion of H_2 increased from 2.42% to 9.22%, while the proportions of CO_2 and CO continued to decline. CH_4 and other hydrocarbon gases predominantly originated from the cleavage of side chains in organic macromolecules, whereas H_2 derived from the polycondensation of H radicals, and CO/CO_2 formed via the fracture of carboxyl groups and oxygen-containing heterocycles. Elevated temperatures further promoted C–C bond cleavage and dehydrogenation reactions (Wang et al., 2022a, 2022b). Fig. 4(f) depicted the ratio of alkanes to olefins within the organic constituents of pyrolysis gas, alongside the variation in the calorific value of the gas across diverse reaction temperatures. It was observable that the alkanes-to-olefins ratio diminished as the temperature rose. The elevation in temperature intensified the secondary reactions, including alkane dehydrogenation and aromatic bond cleavage, which led to the production of olefins. Consequently, this shift resulted in a decrease in the proportion of alkanes and a corresponding increase in the proportion of olefins. Simultaneously, the augmentation in temperature facilitated the thermal cracking of macromolecules, such as gums and asphaltenes, yielding lighter oils and gases, and contributed to a continuous escalation in the proportion of organic components within the pyrolysis gas, thereby causing a concurrent increase in its calorific value (Lai et al., 2016).

3.3. The effect of particle size on the properties and distribution of co-pyrolysates from the mixture

Fig. 5(a) indicated the distribution of co-pyrolysates from the mixture at different particle sizes when reaction temperature was 520 °C, nitrogen flow rate was 0.6 L/min and reaction time was 8 min. The yield of pyrolysis oil of mixtures with a particle size of 0.7–1.0 mm was 16.80 wt.%, whereas the mixture with a particle size <0.2 mm exhibited a yield of 19.78 wt.%, representing a 2.98 wt.% reduction for the larger particle. These results are in line with prior research, confirming that smaller particle sizes enhance the yield of pyrolysis oil (Nazzal, 2008). Fig. 5(b) presented that for particle size <0.2 mm, the relative content and yield of coke deposition were 70.22% and 39.39 wt.%, respectively, 3.85% and 6.45 wt.% lower than those for particle size of 0.7–1.0 mm. This indicated that smaller particle sizes can advance the efficiency of pyrolysis reactions and facilitate the cleavage of organic macromolecular bonds (Tian and Perré, 2023; Xiao et al., 2020).

Fig. 5(c) demonstrated the carbon number distribution of pyrolysis oil across particle size ranges. It was obvious that variations in the particle sizes of the mixture resulted in distinct distributions of carbon number within the pyrolysis oil. Specifically, as the particle size decreased, the proportion of the C_6–C_{12} components augmented from 24.78% to 26.37%. However, the proportion of the C_{13}–C_{20} components remained relatively stable and the proportion of the C_{21+} components decreased from 33.08% to 31.55%. The observed changes were primarily attributed to the influence of particle size on heavy oil components. Smaller particle size enhanced heat transfer efficiency, intensifying secondary reactions of heavy oil, which could facilitate the fragmentation of long-chain aliphatic hydrocarbons and the release of lighter oil components, ultimately shifting the carbon number distribution of pyrolysis oil toward lower-carbon species. Fig. 5(d) presented the relative contents and yields of components in the pyrolysis oil obtained from different mixture particle sizes. It could be concluded that the primary constituent of the pyrolysis oil comprised alkanes, olefins, and phenols. As the particle size decreased from 0.7 to 1.0 mm to <0.2 mm, the relative content of alkanes declined from 54.9% to 51.47%, while olefins increased from 31.49% to 32.94%, and phenols rose from 10.69% to 12.64%. Smaller particle sizes promoted heat transfer efficiency, which lowered the production temperatures of pyrolysis oil and intensified secondary reactions. Especially, elevated heat transfer efficiency could increase cleavage of alkane bonds to result in the formation of olefins and light hydrocarbon gases, and facilitate fragmentation of ether bonds (C–O) and carbonyl groups (C=O) in organic molecules, which together increased the yields of phenols.

Fig. 5(e) exhibited the composition and distribution of pyrolysis gas obtained under various particle sizes. When the particle size decreased from 0.7 to 1.0 mm to <0.2 mm, the proportion of CH_4 increased by 4.82%, H_2 rose by 1.03%, and CO_2 declined by 11.64%. These findings illustrated that smaller particle sizes enhance secondary reactions of fragment long-chain fatty hydrocarbons into light gases (Tian et al., 2016; Xu et al., 2021). Fig. 5(f) presented the ratio of alkanes to olefins and the calorific value of the pyrolysis gas at different particle sizes. It was shown that a decrease in particle size resulted in a reduction in the ratio of alkanes to olefins and an increase in the calorific value of the pyrolysis gas, which was in line with the changing trend of the components of pyrolysis oil, verifying that a smaller particle size led to a higher degree of secondary reactions (Hong et al., 2020).

3.4. The effect of nitrogen flow rate on the properties and distribution of co-pyrolysates from the mixture

Fig. 6(a) presents the distribution of co-pyrolysates from the mixture at different nitrogen flow rates when reaction temperature was 520 °C, particle sizes was 0.7–1.0 mm, and reaction time was 8 min. As the nitrogen flow rate increased, the yield of pyrolysis oil initially rose from 18.60 to 20.30 wt.% and then declined to 17.00 wt.%, while the yields of pyrolysis gas and semi-coke showed minimal variation. At low nitrogen flow rate, inadequate fluidization of the mixture and solid heat carrier hindered heat-transfer and mass-transfer processes, leading to outward

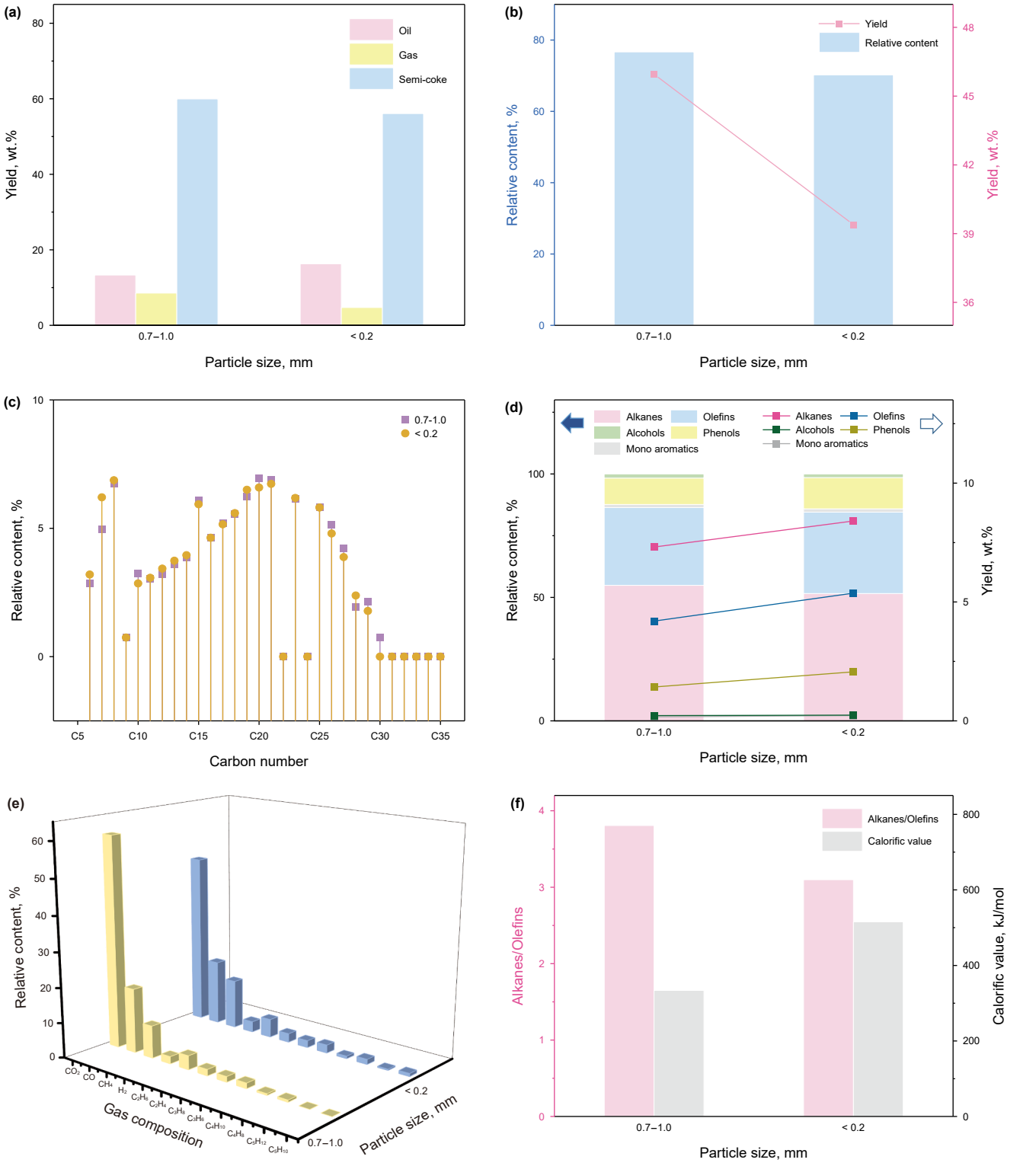

Fig. 5. The effect of particle size on properties and distribution of pyrolysates: **(a)** The distribution of three-phase pyrolysates; **(b)** The relative content and yield of coke deposition; **(c)** The distribution of carbon number in pyrolysis oil; **(d)** The relative content and yield of components in pyrolysis oil; **(e)** The relative content of components in pyrolysis gas; **(f)** The properties of pyrolysis gas.

diffusion of pyrolysates becoming the controlling step. Heavy oil components remained on the mixture surface and within pores, undergoing cracking and coking reactions, resulting in reduced yield of pyrolysis oil and elevated yield of semi-coke (Pan et al., 2022; Wulandari et al., 2020). When the nitrogen flow rate increased from 0.4 to 0.6 L/min, the yield of pyrolysis oil increased by 1.7 wt.%, indicating that improved fluidization enhances the yield of pyrolysis oil by facilitating separation of pyrolysates from the reaction system and reducing coking of hydrogen-deficient components and cracking of long-chain aliphatic hydrocarbons.

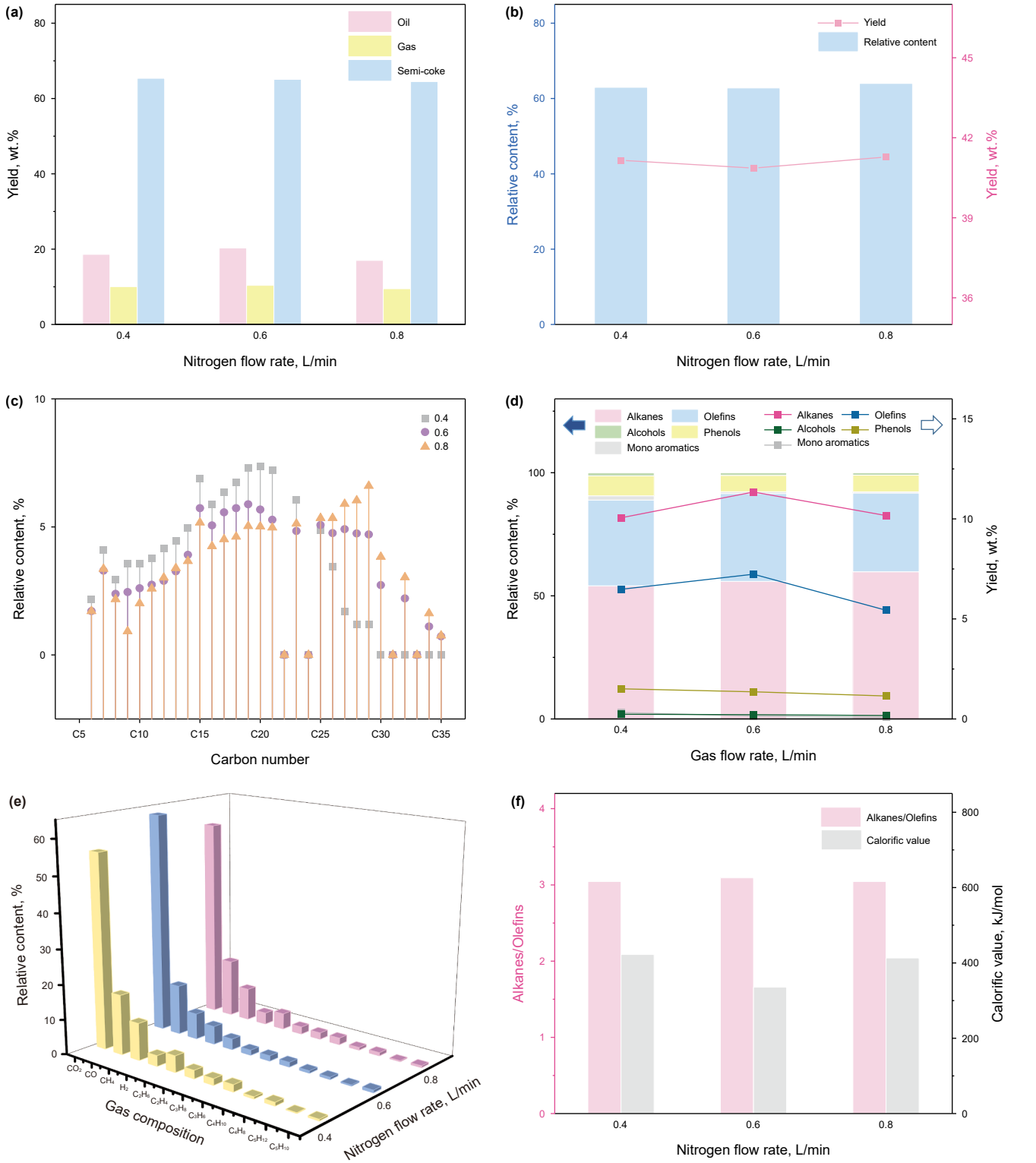

Fig. 6. The effect of nitrogen flow rate on properties and distribution of pyrolysates: **(a)** The distribution of three-phase pyrolysates; **(b)** The relative content and yield of coke deposition; **(c)** The distribution of carbon number in pyrolysis oil; **(d)** The relative content and yield of components in pyrolysis oil; **(e)** The relative content of components in pyrolysis gas; **(f)** The properties of pyrolysis gas.

However, further increasing the flow rate to 0.8 L/min decreased the yield of pyrolysis oil by 3.29 wt.%, attributed to insufficient condensation time in the condensing unit. Fig. 6(b) illustrated that the relative content and yield of coke deposition exhibited negligible variation, consistent with the trends in Fig. 6(a).

Fig. 6(c) depicted the carbon number distribution of pyrolysis oil at varying nitrogen flow rates. As the nitrogen flow rate increased, the proportion of C_6–C_{12} components declined from 24.31% to 15.79%, C_{13}–C_{20} components decreased from 49.99% to 35.64%, and C_{21+} components rose from 25.71% to 48.57%. Overall,

the pyrolysis oil shifted toward a higher carbon number range, indicating that elevated nitrogen flow rates enhanced fluidization of mixture, effectively suppressing secondary reactions of pyrolysis oil (Han et al., 2024). Fig. 6(d) displayed the relative content and yields of components in pyrolysis oil across nitrogen flow rates. Specifically, as the nitrogen flow rate increased, the relative content of alkanes rose by 5.72%, while olefins, aromatic hydrocarbons, and phenols decreased by 2.88%, 1.24%, and 1.33%, respectively. These trends suggested that higher nitrogen flow rates inhibit secondary reactions of alkanes into olefins and the Diels-Alder reaction of olefins into aromatics (Wang et al., 2021), thereby improving quality of pyrolysis oil.

Fig. 6(e) illustrated the relative content of pyrolysis gas across nitrogen flow rates. As the nitrogen flow rate increased, the proportions of CH_4 and H_2 decreased, while CO_2 increased. Fig. 6(f) demonstrated the ratio of alkanes to olefins and calorific value of pyrolysis gas. The ratio of alkane to olefin changed little, but the calorific value peaked at a nitrogen flow rate of 0.4 L/min.

3.5. The effect of heating rate on the properties and distribution of co-pyrolysates from the mixture

Compared to the heating rate of fluidized pyrolysis, the heating rate of Py-GC-MS represented faster. To better elucidate the mechanisms of secondary reactions, a comparative analysis of the pyrolysis oil obtained from both fluidized pyrolysis (slow pyrolysis) and Py-GC-MS (fast pyrolysis) was conducted, with the results presented in Fig. 7.

As shown in Fig. 7(a), the fast pyrolysis oil exhibited a relatively higher proportion of light oil components and a lower proportion of heavy oil components. The fast pyrolysis oil contained 25.82% C_6–C_{12} components, 37.05% C_{12}–C_{20} components, and 36.31% C_{21+} components. In contrast, the corresponding relative content from slow pyrolysis oil were 18.09%, 40.83%, and 41.09%, respectively. In the fast pyrolysis experiments, the extremely high heating rates enabled the mixture to reach the target pyrolysis temperature almost instantaneously, which meant maximized heat and mass transfer efficiencies. Under such rapid energy input, the macromolecular organic frameworks within the mixture including aliphatic side chains, bridging bonds, and unstable functional groups, underwent extensive and uniform cleavage of C–C and C=C bonds. This process was predominantly governed by a free-radical mechanism, generating a large quantity of primary fragments, which were rapidly carried away by the carrier gas from the high-temperature reaction zone and promptly quenched. The extremely short residence time effectively avoided secondary reactions, such as polymerization, recombination, or further cracking of organic frameworks. As a direct result, the pyrolysis oil showed a significantly increased relative abundance of low-molecular-weight components, manifesting as selective enrichment of light aliphatic hydrocarbons, monocyclic aromatics, and small oxygen-containing compounds. In contrast, the formation of long-chain alkanes and PAHs were markedly suppressed, clearly demonstrating the significant regulatory effect of fast pyrolysis conditions on product distribution.

As illustrated in Fig. 7(b), comparative analysis of pyrolysis oil from slow and fast pyrolysis revealed that aliphatic hydrocarbons constitute the main components of the pyrolysis oils under both modes. The combined percentage of alkanes and olefins exceeded 90%, with alkane-to-olefin ratios of 1.57 and 1.59, respectively, indicating a high degree of similarity in hydrocarbon composition. During slow pyrolysis, the prolonged vapor-phase residence time promoted deeper secondary reactions, leading to an increase in the relative content of unsaturated components within the aliphatic hydrocarbons. Under extended thermal exposure, cracking of larger hydrocarbon molecules could result in a certain degree generation of olefins.

Compared with fast pyrolysis, the slow pyrolysis oil exhibited a significant increase in the relative content of phenols, while the relative content of alcohols decreased. The increase in aromatic hydrocarbons could be attributed to aromatization reactions of aliphatic hydrocarbons and Diels-Alder cyclization on high-temperature conditions, which were more likely to occur under longer residence times, thereby promoting the formation of monocyclic aromatics. The production of phenols mainly originated from the thermal cleavage of oxygen-containing functional groups in macromolecular structures of coal, such as ether bonds and hydroxyl-substituted aromatic rings. Owing to the structural complexity of the organic matter in coal, some stable oxygen-containing bridging bonds did not completely break during the primary pyrolysis stage. Under higher energy input and longer duration provided by slow pyrolysis, these precursor structures underwent further bond cleavage, releasing phenolic compounds.

In contrast, alcohols were mainly derived from the removal or decarboxylation of carboxyl and hydroxyl groups on aliphatic side chains. Under fast pyrolysis conditions, volatile products can

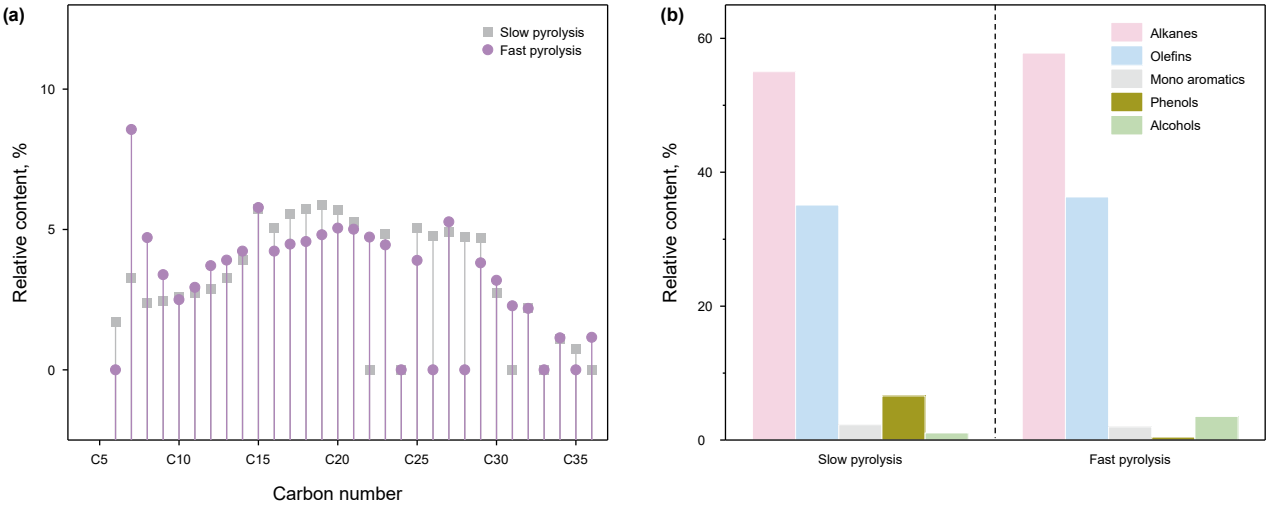

Fig. 7. The composition and distribution of pyrolysis oil from slow pyrolysis and fast pyrolysis: **(a)** The distribution of carbon number; **(b)** The relative content of components.

rapidly escape the reaction system and were largely preserved. However, during slow pyrolysis, due to intensified secondary reactions, the alcohols already formed were more prone to undergo dehydration, homolytic cleavage of C–O bonds, and reforming reactions, converting into olefins, water, and small gaseous molecules.

3.6. The co-pyrolysis mechanism of the mixture

3.6.1. The formation mechanism of phenol

Fig. 8 illustrated the variation in phenolic compounds during the pyrolysis of OS, BC and their mixture. The yield of m-Cresol in pyrolysis oil obtained from OS was 0.23 wt.%, and its relative content amounted to 1.01%. In contrast, the yield of phenols from pyrolysis of BC was relatively high, reaching 2.88 wt.%, and the relative content was as high as 26.98%. Among these phenols, phenol accounted for the highest proportion of 9.46%, followed by 4-methylphenol of 8.68%. The yield of phenols obtained from pyrolysis of mixture was 1.75 wt.%, while the theoretical yield was 1.29 wt.%, which indicated that co-pyrolysis of OS and BC promoted the formation of phenols. The phenols in pyrolysis oil of the mixture were mostly derived from the phenoxy structure in the kerogen of BC.

Fig. 8(b) demonstrated the actual and theoretical yields of several phenols achieved through the pyrolysis of the mixture. The yields of phenol, 4-methylphenol, 2,3-xylenol, and m-ethylphenol showed significant increased while m-cresol formation was suppressed. During the pyrolysis of coal, CaO and Fe_2O_3 had significant influences on the formation and distribution of catechol. Among them, the catalytic performance of CaO was more obvious than that of Fe_2O_3. Moreover, CaO could enhance the generation of m/p-cresol, but Fe_2O_3 cannot (Bai et al., 2014). Alkali and alkaline earth metals inhibited the formation of phenol during BC pyrolysis, because the bivalent metal cation combined with the coke matrix to form cross-links, which could break smaller aromatic ring systems into light gases and condense larger aromatic systems into coke (Li et al., 2000). XRF results in Table 2 revealed that compared with BC, OS contained fewer minerals such as CaO, Fe_2O_3. Since the OS content in the mixture is 60%, the alkali/alkaline earth metal content was significantly lower than that of pure BC. Consequently, he cross-linking density between the bivalent metal cation and the coke matrix decreased during the pyrolysis of the mixture, leading to the release of aliphatic components and smaller aromatic ring systems in tar precursor, thereby increasing the total yield of phenols. As shown in Fig. 9, in the secondary reactions, phenols released from cross-links in semi-coke, and the mixing process inhibited the formation of m-cresol.

3.6.2. The cracking mechanism of organic macromolecules

The experimental results indicated that the effects of reaction temperature, particle size, nitrogen flow rate, and heating rate on properties and distribution of pyrolysates exhibited a high degree of consistency. The underlying mechanism lay in the synergistic regulation of these factors on the residence time of pyrolysis volatiles and the extent of their secondary reactions.

Fig. 9 illustrated the primary and secondary reactions during the co-pyrolysis of the mixture with increasing residence time. Both oil shale and bituminous coal consisted of kerogen macromolecules and inorganic minerals. The inorganic components influenced the pyrolysis process by providing acid sites and the structure of kerogen directly determined the outcome and properties of the pyrolysates. As pyrolysis proceeded, the long-chain aliphatic structures in oil shale firstly cracked into hydrogen radicals and aliphatic chain fragments, attributing to the significantly higher H/C ratio of oil shale compared to bituminous coal, which enabled oil shale to supply a greater quantity of active H radicals. The reticular organic molecular structure of bituminous coal fractured to generate aryl radicals, alkoxy radicals, phenoxy radicals, aliphatic chain fragments, and methyl radicals. Continual collisions among these fragments led to the formation of primary pyrolysates.

With prolonged residence time of volatiles in the high-temperature zone, the degree of secondary reactions in the mixture increased. Long-chain aliphatic hydrocarbons unceasingly underwent β-scission of C–C bonds at high temperatures, producing smaller alkyl radicals and olefins. Through successive steps of dehydrogenation, bond cleavage, and radical recombination, the long-chain aliphatic hydrocarbons were eventually converted into lighter components, which resulted in an increase in gaseous products such as CH_4, C_2H_6, and C_2H_4, while the organic macromolecule in the pyrolysis oil shifted toward lower carbon numbers with a concurrent rise in olefin content. The light gas underwent decomposition and dehydrogenation reactions at high temperatures to produce CH_4 and H_2.

Light olefins and dienes served as important precursors for the formation of large aromatic hydrocarbons via free-radical

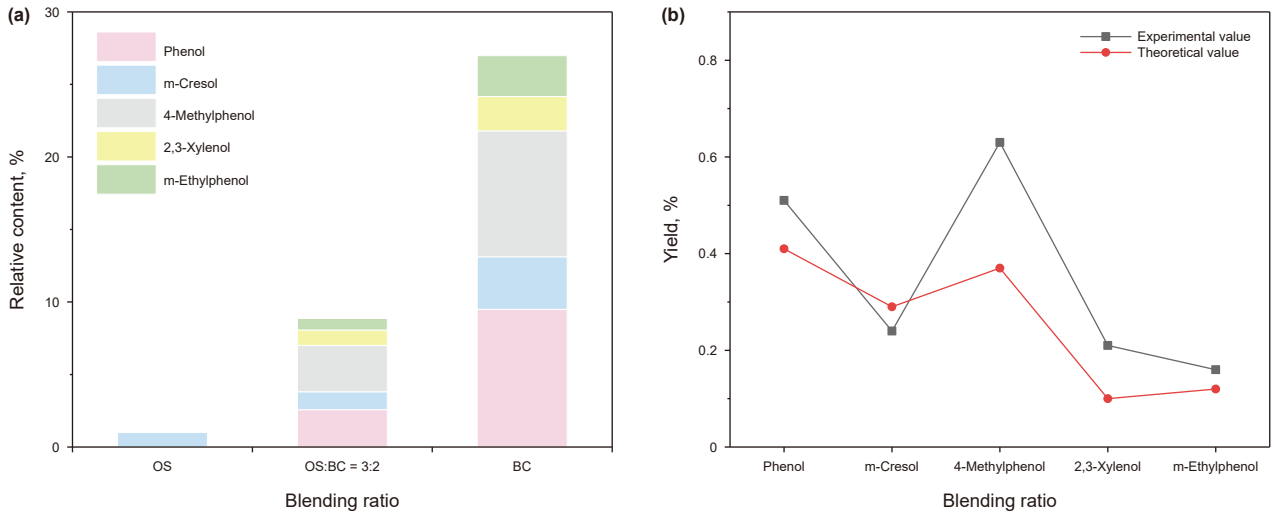

Fig. 8. The effects of co-pyrolysis on phenolic composition in pyrolysis oil: **(a)** The composition of phenols; **(b)** The theoretical and experimental values of each phenol.

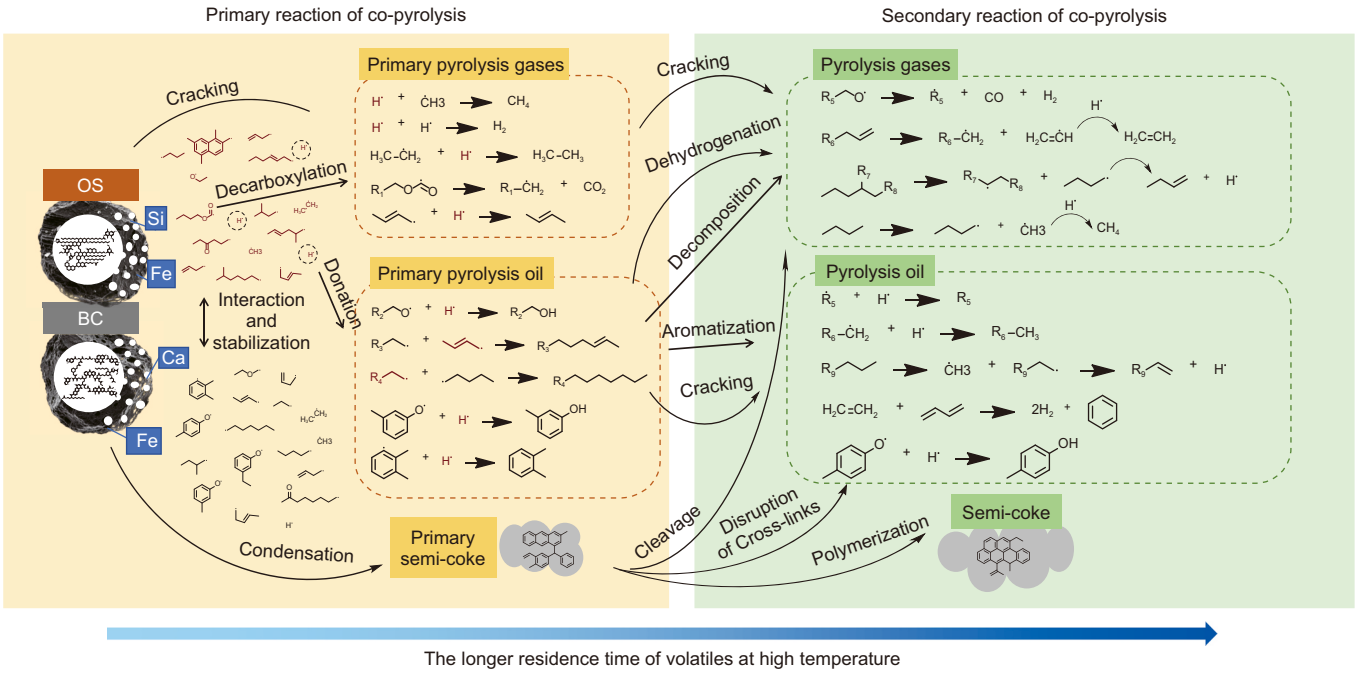

Fig. 9. The co-pyrolysis mechanism of mixture at different residence time.

reactions. For instance, vinyl radicals attacked butadiene through radical addition, followed by a series of cyclization and dehydrogenation to yield benzene and its derivatives. Oxygen-containing functional groups on aliphatic side chains exhibited relatively low thermal stability. They primarily decomposed through homolytic cleavage of C–O bonds, dehydration, or decarbonylation, generating H_2O, CO, and hydrocarbon radicals. In contrast, phenolic –OH groups attached to aromatic rings demonstrated higher thermal stability due to p-π conjugation with the aromatic ring. These groups were typically released as monomers from the macromolecular network of the mixed samples during secondary reactions and becoming significant oxygen-containing components in the pyrolysis oil.

4. Conclusion

In this manuscript, co-pyrolysis of OS and BC was investigated in a fluidized bed, focusing on the effects of temperature, particle size, nitrogen flow rate, and heating rate on properties and distribution of pyrolysates. The co-pyrolysis technology offered a sustainable route for high-value product generation from low-grade carbon sources. The research results are summarized as follows:

(1) Temperature was the most critical parameter. An optimal temperature of 520 °C was identified, maximizing the yield of pyrolysis oil at 20.95 wt.% while suppressing over-cracking. Beyond this point, secondary reactions were intensified, depleting alkanes in the oil from 55.90% to 41.33% and enriching olefins, aromatics, and phenols.
(2) The effects of temperature, particle size, nitrogen gas flow, and heating rate were unified through a single key variable: the residence time of volatiles, which directly governed the severity of secondary reactions.
(3) A clear synergistic effect was quantified. The addition of OS diluted the catalytic metals in the system, which effectively suppressed cross-linking coking and promoted the release of aromatic precursors, which led to a significant increase in the yield of phenols in the oil, from 1.27 wt.% to 1.75 wt.%.
(4) The secondary reactions were dominantly driven by free-radical chain mechanisms, thermodynamically steering the product slate toward stable molecules, including light organic component and stable aromatics, at the expense of the primary oil.

CRediT authorship contribution statement

Dong-Ling Xu: Writing – original draft, Resources, Conceptualization. **Yue Ma:** Writing – review & editing. **Zhi-Jun Fu:** Investigation. **Lu Gong:** Formal analysis. **Ze-Kai Zhang:** Project administration. **Hao-Lun Wang:** Validation. **Jin-Ke Wang:** Methodology. **Feng-Zhi Guo:** Supervision. **Si-Jia Li:** Supervision. **Ke-Xin Zhao:** Software. **Chang-Tao Yue:** Writing – review & editing.

Declaration of competing interest

The authors declare that they have no known competing financial interests or personal relationships that could have appeared to influence the work reported in this paper.

References

Amer, M.W., Aljariri Alhesan, J.S., Marshall, M., et al., 2019. Characterization of Jordanian oil shale and variation in oil properties with pyrolysis temperature. J. Anal. Appl. Pyrolysis 140, 219–226. https://doi.org/10.1016/j.jaap.2019.03.019.
Bai, Y., Yan, L., Li, G., et al., 2014. Effects of demineralization on phenols distribution and formation during coal pyrolysis. Fuel 134, 368–374. https://doi.org/10.1016/j.fuel.2014.05.076.
Bhattacharyya, M., Shadangi, K.P., Purkayastha, R., et al., 2024. Co-pyrolysis of coal and biomass blends: impact of pyrolysis temperature and biomass blending on thermal stability of coal, and composition of pyrolysis products. Process Saf. Environ. Prot. 187, 1010–1021. https://doi.org/10.1016/j.psep.2024.05.037.
Chang, Z., Wang, X., Hao, C., et al., 2023. Non-catalytic and in-situ catalytic co-pyrolysis of Huadian oil shale and microalgae using several additives as catalyst. J. Anal. Appl. Pyrolysis 172, 106012. https://doi.org/10.1016/j.jaap.2023.106012.

Chen, X., Zhao, Y., Liu, L., et al., 2018. Evaluation of chemical structure, pyrolysis reactivity and gaseous products of shenmu coal of different particle sizes. J. Anal. Appl. Pyrolysis 130, 294–304. https://doi.org/10.1016/j.jaap.2017.12.019.
Cui, S., Li, R., Yang, T., et al., 2024. Production of bio-crude from co-pyrolysis of oil shale and peanut shell over semi-coke supported ni catalyst. J. Anal. Appl. Pyrolysis 181, 106618. https://doi.org/10.1016/j.jaap.2024.106618.
Cui, Z., Lu, Y., Cao, R., et al., 2024. Synergistic effect and hydrogen migration during co-pyrolysis of oil shale and cherry pit. Fuel 365, 131275. https://doi.org/10.1016/j.fuel.2024.131275.
Ding, H., Ma, Y., Li, S., et al., 2022. Pyrolytic characteristics of fushun oil shale and its by-products. J. Therm. Anal. Calorim. 147, 5255–5267. https://doi.org/10.1007/s10973-021-10870-8.
Fan, C., Yan, J., Huang, Y., et al., 2015. XRD and TG-FTIR study of the effect of mineral matrix on the pyrolysis and combustion of organic matter in shale char. Fuel 139, 502–510. https://doi.org/10.1016/j.fuel.2014.09.021.
Gao, H.S., Zong, Z.M., Li, J.H., et al., 2021. Characterization of oxygen-containing aromatics in a low-temperature coal tar. Energy Fuel. 35, 283–289. https://doi.org/10.1021/acs.energyfuels.0c02571.
Han, X., Wang, Y., Huang, Y., et al., 2024. Experimental and numerical investigation on the pyrolysis of oil shale particles in a bubbling fluidized bed. J. Anal. Appl. Pyrolysis 179, 106515. https://doi.org/10.1016/j.jaap.2024.106515.
Hong, Z., Zhong, F., Niu, W., et al., 2020. Effects of temperature and particle size on the compositions, energy conversions and structural characteristics of pyrolysis products from different crop residues. Energy 190, 116413. https://doi.org/10.1016/j.energy.2019.116413.
Huang, Y., Li, W., Wu, G., et al., 2017. Comparative analysis of typical low rank coal pyrolysis technology based on a nonlinear programming model. Energy Fuels. 31, 12977–12987. https://doi.org/10.1021/acs.energyfuels.7b02412.
Kareemulla, D., Gusev, S., Bhattacharya, S., et al., 2024. Entrained-flow pyrolysis and (co-)gasification characteristics of Indian high-ash coals. Energy 294, 130732. https://doi.org/10.1016/j.energy.2024.130732.
Kılıç, M., Pütün, A.E., Uzun, B.B., et al., 2014. Converting of oil shale and biomass into liquid hydrocarbons via pyrolysis. Energy Convers. Manag. 78, 461–467. https://doi.org/10.1016/j.enconman.2013.11.002.
Kong, J., Zhao, R., Bai, Y., et al., 2014. Study on the formation of phenols during coal flash pyrolysis using pyrolysis-GC/MS. Fuel Process. Technol. 127, 41–46. https://doi.org/10.1016/j.fuproc.2014.06.004.
Lai, D., Shi, Y., Geng, S., et al., 2016. Secondary reactions in oil shale pyrolysis by solid heat carrier in a moving bed with internals. Fuel 173, 138–145. https://doi.org/10.1016/j.fuel.2016.01.052.
Li, C., Sathe, C., Kershaw, J.R., et al., 2000. Fates and roles of alkali and alkaline earth metals during the pyrolysis of a victorian brown coal. Fuel 79, 427–438. https://doi.org/10.1016/S0016-2361(99)00178-7.
Li, S., Ma, X., Liu, G., et al., 2016. A TG–FTIR investigation to the co-pyrolysis of oil shale with coal. J. Anal. Appl. Pyrolysis 120, 540–548. https://doi.org/10.1016/j.jaap.2016.07.009.
Li, X., Qi, X., Chen, R., et al., 2024. The influence of solid heat carrier load of char on pyrolysis characteristics of pulverized coal in a fluidized bed reactor. Energies 17, 2282. https://doi.org/10.3390/en17102282.
Liu, C., Li, Y., Fan, D., et al., 2025a. In situ catalytic pyrolysis of oily sludge using coal gangue char to produce naphthalene-rich oil and hydrogen-rich gas. Chem. Eng. J. 508, 160953. https://doi.org/10.1016/j.cej.2025.160953.
Liu, N., Huang, H., Feng, J., et al., 2025b. Effects of alkali and alkaline earth metals in biomass on co-pyrolysis characteristics and product distribution of coal and biomass. Fuel 389, 134551. https://doi.org/10.1016/j.fuel.2025.134551.
Liu, Y., Ali Siyal, A., Zhou, C., et al., 2024. Microwave co-pyrolysis of industrial sludge and waste biomass: product valorization and synergistic mechanisms. Chem. Eng. J. 485, 150032. https://doi.org/10.1016/j.cej.2024.150032.
Lu, Y., Wang, Y., Zhang, J., et al., 2020. Investigation on the characteristics of pyrolysates during co-pyrolysis of zhundong coal and changji oil shale and its kinetics. Energy 200, 117529. https://doi.org/10.1016/j.energy.2020.117529.
Ma, C., Zhao, Y., Lang, T., et al., 2023. Pyrolysis characteristics of low-rank coal in a low-nitrogen pyrolysis atmosphere and properties of the prepared chars. Energy 277, 127524. https://doi.org/10.1016/j.energy.2023.127524.
Miandad, R., Nizami, A.S., Rehan, M., et al., 2016. Influence of temperature and reaction time on the conversion of polystyrene waste to pyrolysis liquid oil. Waste Manag. 58, 250–259. https://doi.org/10.1016/j.wasman.2016.09.023.
Miao, Z., Wu, G., Li, P., et al., 2012. Investigation into co-pyrolysis characteristics of oil shale and coal. Int. J. Min. Sci. Technol. 22, 245–249. https://doi.org/10.1016/j.ijmst.2011.09.003.
Nazzal, J.M., 2008. The influence of grain size on the products yield and shale oil composition from the pyrolysis of sultani oil shale. Energy Convers. Manag. 49, 3278–3286. https://doi.org/10.1016/j.enconman.2008.03.028.
Niu, M., Pan, L., Ji, P., et al., 2024. A preliminary study on the co-hydrogenation process of coal tar and bio-oil. React. Kinet. Mech. Catal. 137, 1667–1682. https://doi.org/10.1007/s11144-024-02614-0.
Nyoni, B., Hlangothi, S.P., 2023. Co-pyrolysis of low-grade bituminous coal and algal biomass in a rotary kiln: effect of coal/algae ratio and kiln temperature on the yield and composition of the resultant oils. J. Anal. Appl. Pyrolysis 171, 105950. https://doi.org/10.1016/j.jaap.2023.105950.
Pan, R., Zan, Y., Debenest, G., 2022. Oil production from waste polyethylene and polystyrene co-pyrolysis: interactions of temperature and carrier gas flow rate. J. Environ. Chem. Eng. 10, 107555. https://doi.org/10.1016/j.jece.2022.107555.
Qian, Y., Zhan, J., Yu, Y., et al., 2019. CFD model of coal pyrolysis in fixed bed reactor. Chem. Eng. Sci. 200, 1–11. https://doi.org/10.1016/j.ces.2018.12.064.
Röpke, G., Peyrer, H., 1980. Selected contributions to the discussion development of a new lurgi gasifier type Ruhr 100. In: Oils and Gases from Coal. Pergamon, pp. 265–267. https://doi.org/10.1016/B978-0-08-025678-8.50021-X.
Shi, W., Wang, Z., Song, W., et al., 2017. Pyrolysis of Huadian oil shale under catalysis of shale ash. J. Anal. Appl. Pyrolysis 123, 160–164. https://doi.org/10.1016/j.jaap.2016.12.011.
Shu, Y., Liu, B., Zhang, H., et al., 2025. Process design and optimization on upgrading and utilization of ultra-high-quality oil shale by pyrolysis. Fuel 390, 134675. https://doi.org/10.1016/j.fuel.2025.134675.
Song, Y., Lei, S., Li, J., et al., 2021. In situ FT-IR analysis of coke formation mechanism during co-pyrolysis of low-rank coal and direct coal liquefaction residue. Renew. Energy 179, 2048–2062. https://doi.org/10.1016/j.renene.2021.08.030.
Stelmakh, G.P., Tyagunov, B.I., 1986. Utilization of shales for power generation and processing: method of producing power-generation and engine fuels. Nat. Resour. Forum 10, 231–238. https://doi.org/10.1111/j.1477-8947.1986.tb00087.x.
Tian, B., Qiao, Y., Tian, Y., et al., 2016. Investigation on the effect of particle size and heating rate on pyrolysis characteristics of a bituminous coal by TG–FTIR. J. Anal. Appl. Pyrolysis 121, 376–386. https://doi.org/10.1016/j.jaap.2016.08.020.
Tian, Y., Perré, P., 2023. Effects of particle size on the pyrolysis of spruce and poplar: thermogravimetric analyses, DAEM modelling, validation, and prediction of secondary charring. Biomass Bioenergy 176, 106913. https://doi.org/10.1016/j.biombioe.2023.106913.
Wang, F., Gao, N., Quan, C., et al., 2022a. Product distribution from oil sludge and waste tires under high pressure pyrolysis. Fuel 311, 122511. https://doi.org/10.1016/j.fuel.2021.122511.
Wang, J., Jiang, J., Ding, J., et al., 2021. Promoting diels-alder reactions to produce bio-BTX: co-aromatization of textile waste and plastic waste over USY zeolite. J. Clean. Prod. 314, 127966. https://doi.org/10.1016/j.jclepro.2021.127966.
Wang, L., Gao, C.H., Xiong, R.Y., et al., 2024. Development review and the prospect of oil shale in-situ catalysis conversion technology. Pet. Sci. 21, 1385–1395. https://doi.org/10.1016/j.petsci.2023.08.035.
Wang, L., Zhang, Y.F., Zou, Run, et al., 2025. Applications of molecular dynamics simulation in studying shale oil reservoirs at the nanoscale: advances, challenges and perspectives. Pet. Sci. 22, 234–254. https://doi.org/10.1016/j.petsci.2024.09.023.
Wang, W., Lemaire, R., Bensakhria, A., et al., 2022b. Review on the catalytic effects of alkali and alkaline earth metals (AAEMs) including sodium, potassium, calcium and magnesium on the pyrolysis of lignocellulosic biomass and on the co-pyrolysis of coal with biomass. J. Anal. Appl. Pyrolysis 163, 105479. https://doi.org/10.1016/j.jaap.2022.105479.
Wang, W., Ma, Y., Li, S., et al., 2016. Pyrolysis characteristics of longkou oil shale under optimized condition. J. Therm. Anal. Calorim. 125, 983–990. https://doi.org/10.1007/s10973-016-5452-4.
Wu, L., Liu, J., Xu, P., et al., 2022. Biomass hydrogen donor assisted microwave pyrolysis of low-rank pulverized coal: optimization, product upgrade and synergistic mechanism. Waste Manag. 143, 177–185. https://doi.org/10.1016/j.wasman.2022.02.020.
Wu, Y., Tao, S., Wang, Z., et al., 2024. Effect of pyrolysis atmospheres on gaseous products evolution of coal pyrolysis at high temperature. Fuel 366, 131336. https://doi.org/10.1016/j.fuel.2024.131336.
Wulandari, Y.R., Chen, S.S., Hermosa, G.C., et al., 2020. Effect of N2 flow rate on kinetic investigation of lignin pyrolysis. Environ. Res. 190, 109976. https://doi.org/10.1016/j.envres.2020.109976.
Xiao, R., Yang, W., Cong, X., et al., 2020. Thermogravimetric analysis and reaction kinetics of lignocellulosic biomass pyrolysis. Energy 201, 117537. https://doi.org/10.1016/j.energy.2020.117537.
Xiong, C., Chen, J., Xu, R., et al., 2025. Pyrolysis characteristics and mechanism of oil shale in the songliao basin of China. Fuel 386, 134251. https://doi.org/10.1016/j.fuel.2024.134251.
Xu, F., Chu, M., Chang, Z., et al., 2021. Sulfur release and transformation during the pyrolysis of lignite with different particle sizes. J. Anal. Appl. Pyrolysis 156, 105162. https://doi.org/10.1016/j.jaap.2021.105162.
Zhai, M., Wang, X., Zhang, Y., et al., 2015. Characteristics of rice husk tar secondary thermal cracking. Energy 93, 1321–1327. https://doi.org/10.1016/j.energy.2015.10.029.
Zhai, Y., Yang, T., Zhang, Y., et al., 2023. Co-pyrolysis characteristics of raw/torrefied corn stalk and oil shale. J. Anal. Appl. Pyrolysis 171, 105967. https://doi.org/10.1016/j.jaap.2023.105967.
Zhang, J., Van De Vijver, R., Amghizar, I., et al., 2022. Combined catalytic and pyrolytic coking model for steam cracking of hydrocarbons. Ind. Eng. Chem. Res. 61, 3917–3927. https://doi.org/10.1021/acs.iecr.1c05036.
Zhang, Y., Zhu, J., Wang, X., et al., 2023. Mechanism of sulfur migration and conversion in pyrolysis/combustion staged conversion process of high sulfur coal. J. Anal. Appl. Pyrolysis 172, 106026. https://doi.org/10.1016/j.jaap.2023.106026.
Zhao, Y., Guo, S., Shao, C., et al., 2021. Combined impacts of intrinsic alkali and alkaline earth metals and chemical structure on reactivity of low-rank coal char: new explanation for the role of water-soluble AAEMs during pyrolysis and gasification. Fuel 305, 121405. https://doi.org/10.1016/j.fuel.2021.121405.
Zhou, H., Li, H., Duan, R., et al., 2020. An integrated scheme of coal-assisted oil shale efficient pyrolysis and high-value conversion of pyrolysis oil. Energy 196, 117106. https://doi.org/10.1016/j.energy.2020.117106.
Zhu, Y., Li, C., Cao, H., et al., 2025. Effects of spatial distribution of tar-rich coal and oil shale and primary factors on product characteristics during microwave co-pyrolysis. Fuel 385, 134085. https://doi.org/10.1016/j.fuel.2024.134085.